Decoding temporal interpretation of the morphogen Bicoid in the early *Drosophila* embryo

Anqi Huang[1*], Christopher Amourda[1*], Shaobo Zhang[1], Nicholas S. Tolwinski[2,3], and Timothy E. Saunders[1,3,4]

[1]Mechanobiology Institute, National University of Singapore, T-Lab, 5A Engineering Drive 1, Singapore 117411
[2]Division of Science, Yale-NUS College, 12 College Ave West, #01-201, Singapore 138610
[3]Department of Biological Sciences, National University of Singapore, 14 Science Drive 4, Singapore 117543
[4]Institute for Molecular and Cell Biology, Agency for Science Technology and Research, 61 Biopolis Dr, Singapore 138673
* These authors contributed equally
Correspondence: dbsste@nus.edu.sg

SUMMARY

Morphogen gradients provide essential spatial information during development. Not only the local concentration but also duration of morphogen exposure is critical for correct cell fate decisions. Yet, how and when cells temporally integrate signals from a morphogen remains unclear. Here, we use optogenetic manipulation to switch off Bicoid-dependent transcription in the early *Drosophila* embryo with high temporal resolution, allowing time-specific and reversible manipulation of morphogen signalling. We find that Bicoid transcriptional activity is dispensable for embryonic viability in the first hour after fertilization, but persistently required throughout the rest of the blastoderm stage. Short interruptions of Bicoid activity alter the most anterior cell fate decisions, while prolonged inactivation expands patterning defects from anterior to posterior. Such anterior susceptibility correlates with high reliance of anterior gap gene expression on Bicoid. Therefore, cell fates exposed to higher Bicoid concentration require input for longer duration, demonstrating a previously unknown aspect of morphogen decoding.

INTRODUCTION

Morphogens are molecules distributed in spatial gradients that provide essential positional information in the process of development (Turing, 1990; Wolpert, 1969). By activating differential gene expression in a concentration-dependent manner, morphogens instruct the cells to adopt proper cell fates according to their positions in the developing embryos or tissues (Gurdon and Bourillot, 2001; Neumann and Cohen, 1997). The impact of a morphogen gradient on a developing system depends on two characteristics: first, its information capacity in terms of how many distinct cell types it has an effect on; second, its transferring precision – in essence, how reproducible cell fates are in different individuals at given positions. Each of these characteristics depends not only on the local concentration of morphogen molecules that the cells interpret, but also temporal components of such interpretation.

The temporal pattern of morphogen interpretation has been demonstrated in several vertebrate developing systems. Harfe et al. first proposed that the length of time of morphogen signalling is critical for correct cell fate specification. They found that during mouse limb development, cells exposed to Sonic Hedgehog (Shh) morphogen for longer time develop into digits of more posterior identity (Harfe et al., 2004). Similarly, in chick neural tube formation the duration of Shh activity is translated into different cell types along the dorso-ventral axis (Dessaud et al., 2007). In comparison, in fish dorso-ventral patterning it is not the duration but the timing of BMP signaling that is important for correct cell fate determination (Tucker et al., 2008). While in some cases the temporal integration of morphogen signaling is carried out by genetic feedback loops (Dessaud et al., 2010), in many other systems the underlying mechanism has not been unveiled.

52 As the first protein identified to function as a morphogen, Bicoid (Bcd) patterns the cells
53 along the antero-posterior axis in the early embryo of the fruitfly, *Drosophila melanogaster*
54 (Driever et al., 1989). Bcd is maternally deposited and localized at the anterior pole of the
55 embryo in the form of mRNA (Frohnhöfer and Nüsslein-Volhard, 1986). This localized
56 mRNA is further translated upon fertilization, forming a protein gradient with exponential
57 decay in concentration along the antero-posterior axis. Fundamentally acting as a
58 transcription factor, Bcd activates different genes, with the more anteriorly expressed genes
59 having higher Bcd binding affinity (Struhl et al., 1989). Quantitative studies have shown that
60 the Bcd gradient is highly dynamic, with nuclear Bcd concentration constantly changing
61 throughout the first 13 rounds of syncytial cell divisions (Little et al., 2011). It has been
62 suggested that precise positional information endowed by Bcd gradient at one single time
63 point suffices to distinguish neighbor cell identities (Gregor et al., 2007a). However, recent
64 results have motivated intense debate over what is the exact time window when the
65 information carried by Bcd is interpreted (Bergmann et al., 2007; Gregor et al., 2007b; Liu et
66 al., 2013; Lucchetta et al., 2005).
67
68 To address this question, fast and reversible temporal manipulation of Bcd activity is required.
69 In this study, we have developed an optogenetic tool to control Bcd-dependent transcription
70 in the early *Drosophila* embryo with high temporal resolution. Using this tool, we provide a
71 detailed dissection of the temporal components of Bcd decoding *in vivo*. The results unveil an
72 unexpected temporal pattern of Bcd action – cell fates determined by higher Bcd
73 concentration require Bcd for longer duration, while cells experiencing lower Bcd dosage
74 commit to correct fates at earlier developmental stages. Further combining temporal
75 perturbation with quantitative analyses, we find that the differential expression kinetics of
76 target genes can partly explain the mechanism underlying such temporal interpretation.

77 **RESULTS**

78 **Precise temporal control of Bcd-dependent transcription via optogenetic manipulation**

79 We built a light-responsive construct to switch off Bcd-dependent transcription by fusing the
80 optogenetic cassette cryptochrome 2 (CRY2) together with mCherry (mCh) to the N-terminus
81 of Bcd (Kennedy et al., 2010) (Figure 1A). We used standard P-element transformation to
82 insert this CRY2::mCh::Bcd construct at different genomic loci generating diverse fly lines
83 expressing this fusion protein at various levels under the control of the endogenous bcd
84 regulatory sequences.

85

86 We find that in the dark, CRY2::mCh::Bcd transgenics rescues the absence of endogenous
87 Bcd. The expression patterns of four gap genes – *hunchback* (*hb*), *giant* (*gt*), *krüppel* (*kr*) and
88 *knirps* (*kni*) – are reminiscent of wild-type embryos when the light-responsive Bcd construct
89 is expressed in an otherwise *bcd* mutant background (Figures 1B-1E). These embryos
90 hatched as healthy larvae (Figure 1F). In comparison, embryos illuminated with blue light
91 during the first 2.5 hours after egg deposition show severe defects in the anterior, Bcd-
92 dependent, expression domains of *hb*, *gt* and *kni*, while their posterior counterparts remain
93 intact (Figures 1G, 1H, and 1I). Furthermore, the Kr band shifts anteriorly when compared to
94 the pattern observed in the dark (Figures 1E and 1J, arrowheads). Illuminated embryos fail to
95 develop the head and thorax structures (Figure 1K), resembling the *bcd* knockout phenotype
96 (Figure 1L). Altogether, these data indicate that the blue light-induced conformational change
97 of CRY2 inhibits Bcd-dependent gene expression. We quantified the Bcd gradient under dark
98 and illuminated conditions (Figures 1M and 1N) and observed no significant change in Bcd
99 profile (Figure 1O), showing that the spatial distribution of Bcd molecules is not affected by
100 our manipulation. Besides acting as a transcription factor, Bcd also represses translation of
101 Caudal (Cad) mRNA at the anterior region of the embryo. Remarkably, we saw no shift in

102 Cad gradient in illuminated embryos when compared to those in the dark (Figures 1P-1R),
103 suggesting that light-induced conformational changes did not alter the translation inhibitory
104 capability of Bcd in the cytoplasm. This allows us to dissociate transcriptional and
105 translational roles of Bcd.
106
107 Next we tested whether CRY2::mCh::Bcd under illumination inhibits transcription in a
108 dominant negative manner. We selected two fly lines expressing CRY2::mCh::Bcd at
109 comparatively lower and higher levels in a *bcd* wild-type background, denoted by $CRY2^{low}$
110 and $CRY2^{high}$, respectively (Figures S1A and 1B) and utilized the MS2 system to visualize
111 the transcriptional activity of the Bcd target gene *hb* (Garcia et al., 2013; Lucas et al., 2013).
112 Compared to wild-type embryos - where transcriptional activity of *hb* in the Bcd-dependent
113 anterior domain persists throughout the interphase of nuclear cycle (n.c.) 13 (7.1 ± 3.2 min;
114 Figures 2A and 2B, Movie S1) - $CRY2^{low}$ embryos show significantly reduced transcriptional
115 persistence when illuminated with a 488 nm laser (3.6 ± 1.1 min; Fig.2a, c). Such an
116 inhibitory effect becomes more prominent in $CRY2^{high}$ embryos (3.0 ± 0.5 min, Figures 2A
117 and 2D). The transcription of the posterior *hb* domain is Bcd-independent and, reassuringly,
118 we do not observe any inhibitory effect in this domain (4.3 ± 2.0 min, 5.2 ± 3.3 min, and 4.2
119 ± 2.0 min in control, $CRY2^{low}$, and $CRY2^{high}$, respectively; Figure 2E). Further, the inhibitory
120 effect for the same genetic background and illumination conditions is uniform along the AP
121 axis (Figures S1C and S1D). As parallel evidence, ChIP-qPCR experiments show comparable
122 CRY2::mCh::Bcd binding in dark or light to native Bcd binding sites (Figure 2F), with no
123 noticeable unspecific DNA binding caused by light-induced conformational changes (Figure
124 2G).
125 We then explored the effect of tuning the inhibition of Bcd-dependent transcription by
126 varying the blue-light illumination intensity. We illuminated embryos with blue light at

127 different powers (0.04, 0.4 and 4 mW) during the hour prior to gastrulation. We used the
128 Even-skipped (Eve) pattern, where Eve stripes 1 and 2 are Bcd-dependent and more posterior
129 stripes are Bcd-independent as a readout of Bcd activity (Frasch and Levine, 1987;
130 Stanojevic et al., 2016). In a WT background, low power illumination (0.04 mW) causes a
131 moderate reduction and a slight anterior shift of the Eve stripes 1 and 2 expression (Figures
132 2H and 2I). Increasing light power further decreases the expression level of the first two Eve
133 stripes (Figures 2J and 2K). When expressed in a *bcd* null background, CRY2::mCh::Bcd
134 completely inhibits the expression of the anterior two Eve stripes, even at the lowest light
135 power tested (Figures 2L and 2O).
136
137 Putting the above results together, blue light illumination induces a light-sensitive
138 conformational change of the N-terminal CRY2, resulting in the inhibition of Bcd-dependent
139 target gene transcription by, potentially, hindering the assembly of the transcription
140 machinery. CRY2::mCh::Bcd under illumination competes with wild-type Bcd protein for
141 binding to the native Bcd DNA binding sites, therefore acting as a dominant negative
142 transcription factor. This inhibitory effect was stronger in a *bcd* null background, likely due
143 to the lack of competitive binding. These effects were reversible upon returning to a dark
144 state (see results below and references Guglielmi et al., 2015; Kennedy et al., 2010). Finally,
145 the light-induced conformational change does not affect Bcd's role in translational repression
146 of Cad mRNA. This may be one of the reasons that gap gene expression in illuminated
147 embryos does not perfectly recapitulate that in *bcd* null embryos, where both Bcd
148 transcriptional and translational effects are lost (Figure S2).
149

150 **Persistent Bcd transcription activity is indispensable to embryonic viability**

151 Bcd confers robust cell fate decisions by activating hierarchical segmentation gene networks
152 (Jaeger et al., 2004; Kraut and Levine, 1991; Manu et al., 2009). Previous studies have shown
153 that only at early n.c. 14 is the absolute Bcd concentration interpreted as positional
154 information. In late n.c. 14, on the contrary, expression boundaries of downstream genes are
155 subjected to cross-regulation and the Bcd gradient is believed to no longer be important (Liu
156 et al., 2013). To determine whether Bcd-dependent transcription in late n.c. 14 is actually
157 irrelevant for cell fate determination, we collected embryos laid by females expressing
158 CRY2::mCh::Bcd in a *bcd* null background ($CRY2^{high}$, bcd^{-}; in all following experiments
159 unless otherwise stated) and illuminated them before the initiation of gastrulation for time
160 windows ranging from 10 to 60 minutes (Figure 3A). Surprisingly, 10 minutes of
161 illumination at the end of n.c. 14 is sufficient to induce embryonic lethality. Cuticle
162 preparation of these non-hatched embryos shows defective mouthparts, in particular the
163 pharynx (Figures 3B and 3C, arrows). In addition, the structures between mouth hooks and
164 cephalo-pharyngeal plates are missing (Figure 3C, arrowhead). Thirty minutes of
165 illumination causes further deterioration in mouth development, with minimal mouth skeleton
166 visible (Figure 3D). Extending the illumination window depletes all mouthparts (Figures 3E
167 and 3F), with the most severe phenotypes observed when illumination encompasses both n.c.
168 13 and n.c. 14. Under this condition, all thorax segments are lost, with only abdominal
169 denticle belts remaining (Figure 3F).

170

171 Transcripts of Bcd target genes have been detected using *in situ* hybridization at time points
172 as early as n.c. 7 (Ali-Murthy and Kornberg, 2016). We tested whether such early Bcd-
173 dependent transcription was essential for embryonic viability by illuminating embryos during
174 early developmental stages (*i.e.* before n.c. 14) and reverting them later to dark conditions to

175 recover Bcd-dependent transcription. We find that a 30-minute illumination window
176 spanning n.c. 11~13 results in severe patterning defects (Figure 3G), phenocopying the
177 embryos illuminated during n.c. 13 and 14 (Figure 3F). This suggests that Bcd-dependent
178 transcription before n.c. 14 is indispensable for initiating its downstream gene cascade.
179 Shifting the 30-minute illumination period to 10 minutes earlier results in the recovery of
180 proper thoracic segment patterning (Figure 3H, arrowhead). As the illumination time window
181 is shifted sequentially earlier, more thorax and mouthparts are successively recovered
182 (Figures 3I-3K). Last, when the illumination time window is shifted before n.c. 10 (Figure
183 3K), the cuticle patterns become equivalent to those of embryos developed in the dark
184 (Figure 3B) and, moreover, the larval hatchability reaches that of dark conditions.
185
186 These temporal perturbation experiments reveal that persistent Bcd-dependent transcription
187 activity from n.c.10 is required for robust embryonic patterning, and ultimately embryonic
188 viability. In contrast, formation of the more posterior, thoracic segments is only perturbed
189 when extended illumination covers n.c.13, the critical time window for properly initiating the
190 downstream gene cascade.
191
192 **Anterior cell fates require Bcd-dependent transcription for longer duration**
193 Deprivation of Bcd-dependent transcription in late blastoderm stages leads to embryonic
194 lethality, due to errors in cell fate determination. To determine which cell fates are altered by
195 the lack of Bcd function (Figure 4A), we fixed illuminated CRY2^{high}, *bcd*$^{-}$ embryos at the end
196 of germband extension (GBE, 4 hours after gastrulation initiates) and analyzed the expression
197 of Engrailed (En) and various Hox genes. The most anterior morphological features that can
198 be observed at GBE are the clypeolabrum lobe at the very tip of the embryo and the
199 invagination of stomodeum (Figure 4B, red and orange dots, respectively). Blue-light

200 illumination for 10 minutes before gastrulation impairs the formation of these very anterior
201 structures while the expression of the more posterior En stripes remains intact (Figure 4C).
202 Extending illumination to 30 minutes prior to gastrulation, we observe the loss of the next
203 two En stripes marking the mandibular (Mn) and maxillary (Mx) segments (Figure 4D).
204 Concomitantly, we observe diminished expression of Deformed, a Hox gene that controls
205 morphogenesis of these same Mn and Mx segments (Figure 4D'). This suggests that
206 presumptive Mn and Mx cells commit to alternative cell fates. Similarly, 50 minutes of
207 illumination prior to gastrulation results in the loss of expression of Sex Comb Reduced (Scr),
208 the hox gene that regulates development of the labial segment (Figures 4E' and 4E''). This
209 correlates with the loss of the En stripe marking this very same segment (Figure 4E). Further
210 extending illumination, we observe that anterior cells adopt posterior cell fates, reflected in
211 the ectopic expression of Ultrabithorax (Ubx) and Abdomen-B (Abd-B) in anterior regions
212 (Figures 4E'', 4F'' and S3F'', arrows). In the most severe case, we see that all En segments
213 from the anterior to the third thorax (T3) are missing (Figure 4F).
214
215 Sequential disappearance of En stripes from anterior to posterior correlates with prolonged
216 illumination at the end of the blastoderm stage. This evidence shows that more anterior cell
217 fates require Bcd-dependent transcription to persist until the very end of n.c. 14. In contrast,
218 cells in more posterior regions undergo correct fate decisions at earlier stages, regardless of
219 the Bcd transcription activity at later time points.
220
221 **Temporal dissection of Bcd target gene expression**
222 To gain deeper insight into the molecular basis of the spatio-temporal readout dependence on
223 Bcd, we investigated how deprivation of Bcd-dependent transcription at different time
224 windows affects downstream gap gene expression. To this end, we inhibited Bcd-dependent

225 transcription at precise time windows (Figure 5A), then fixed these embryos at the end of the
226 blastoderm stage, and stained them for a range of gap genes.
227
228 First, we looked at the gap gene *hb*. Our live imaging (Figures 2A-2E) reveals that
229 illumination significantly reduces the transcription activity of the *hb* anterior domain.
230 Surprisingly, illumination during the last 30 minutes of the blastoderm stage does not affect
231 Hb in neither protein level nor boundary position (Figure 5B), indicating that Hb expression
232 is independent of the newly synthesized mRNA in the last 30 minutes of n.c. 14. This shows
233 that the Hb protein level remains stable once the *hb* mRNA amount has exceeded a certain
234 threshold value. However, extending illumination throughout n.c. 14 (or even earlier) results
235 in deviations of the Hb anterior pattern (Figures 5B, arrows; and S4B4). It has previously
236 been reported that the Hb pattern due to the activity of the *hb* stripe enhancer at the posterior
237 border evolves during n.c. 14 from a shallow and broad gradient to a steep and sharp one
238 (Perry et al., 2011, 2012). Here, we show that the mRNA synthesized prior to n.c. 14 is
239 sufficient to support the formation of the broad gradient, as demonstrated by the Hb
240 expression profile in embryos illuminated throughout cycle 14 (Figure 5B, curve 4).
241 Transcriptional activity in the first 15 minutes of n.c. 14 is hence critical for precise
242 formation of the wild-type Hb expression profile, at both anterior and posterior (driven by the
243 stripe enhancer) borders. Further, continuous illumination throughout n.c. 13 and n.c. 14
244 severely impairs the anterior Hb expression level (Figures 5C and S4B5), showing that
245 mRNA synthesized during n.c. 13 contributes significantly to the final Hb pattern.
246 Interestingly, recovering the transcriptional activity during the last 30 minutes of n.c. 14 by
247 reverting the embryos to the dark, results in a partial rescue of Hb anterior expression (Figure
248 5C, arrow), supporting the presence of a *hb* mRNA threshold. Nevertheless, transcription
249 activity in late n.c. 14 fails to recover the stripe enhancer activity (Figure 5C, curve 1 and 6),

250 potentially due to shifted borders of posterior repressive factors. Next, we tested the
251 contribution of *hb* transcription prior to n.c.13. Illumination during n.c. 10-12 results in a
252 steep but narrow Hb gradient, where the posterior boundary shifts anteriorly by ~10% EL
253 (Figure 5D). Illumination carried out before n.c. 11 results in a recovery of the shape of the
254 Hb gradient when comparing to that of dark conditions, although the posterior border is still
255 anteriorly shifted by 5% EL (Figures 5D, curve 8 and 5E-F, anterior shift indicated by red
256 dashed line). This suggests that the production of zygotic *hb* transcription during n.c. 10-12
257 plays a critical role in *hb* auto-regulation, affecting the boundary positions of the mature Hb
258 pattern. Therefore, we can temporally dissect Bcd-dependent activation of Hb, including
259 separating the contributions from different enhancers.
260
261 The expression of the gap genes Kr (58-45% EL) and Kni (45-37% EL) is subjected to fine-
262 tuning by Bcd-dependent transcription (in combination with Hb) (Hoch et al., 1991;
263 Hülskamp et al., 1990). We find that the anterior boundary of Kr shows very high sensitivity
264 to Bcd transcriptional inhibition - 20 minutes of illumination during the end of n.c. 14 causes
265 an anterior shift by 3% EL, slightly widening the Kr domain (Figure 5G, 2, blue dot). Both
266 the anterior and posterior borders of the Kr expression domain shift anteriorly upon
267 illumination conditions 4, 5 and 6 (Figure 5G), correlating with the shift of the Hb boundary
268 (Figures 5B curve 4 and 5C, curves 5 and 6). The strongest anterior shift of Kr boundaries is
269 observed when embryos are reverted to dark after early illumination (Figure 5G, curve 6 and
270 7), as repressive Hb expression is anteriorly shifted (Figures 5C, curve 6 and 5D, curve 7)
271 while Bcd transcriptional activity is recovered. The Kni anterior boundary shifts in
272 correspondence with the posterior Kr boundary shifts, while its posterior boundary is much
273 less sensitive (Figure 5H). In summary we find that the more anterior expression boundaries
274 are located, the more susceptible they are to temporal inhibition of Bcd-dependent

275 transcription. Further, we find that a tight temporal interplay between Bcd and Hb is required
276 for the precise positioning of gap gene expression boundaries.
277
278 **Spatio-temporal atlas of Bcd decoding**
279 We now construct a novel spatio-temporal atlas of Bcd-dependent gene transcription in the
280 early *Drosophila* embryo, with clear time windows for gene activation (Figure 6A). A
281 minimal 20-minute illumination at the end of n.c. 14 abolishes the expression of the Knirps
282 anterior domain (Kni1) capping the tip of the embryo (Figures 6B and 6B'), as well as the
283 first Giant stripe (Gt1) (Figures 6C and 6C'). Extending the Bcd inactivation across n.c. 14
284 further inhibits the gap gene expression domains located slightly more posterior,
285 Orthodenticle (Otd) and the second Gt stripe (Gt2) (Figures 6C'', 6D and 6D'). Recovery of
286 transcription activity in late stages fails to rescue the expression of most of these anterior gap
287 gene domains (Figures S4C6, S4D6 and S4F6). When Bcd-dependent transcription is
288 inhibited during n.c. 10-12 and then embryos returned to dark from n.c. 13, the time window
289 for transcriptional recovery (approximately 1 hour) is insufficient to rescue the expression
290 patterns of Kni1, Gt1 and Otd (Figures S4C7, S4D7, S4F7). This supports a mechanism
291 whereby Bcd-dependent transcription serves a priming role prior to n.c. 13 to activate
292 anterior segmentation genes at later stages. Such a priming role is stage-specific, as it is not
293 compensated by late recovery of Bcd transcriptional activity. In comparison, illumination for
294 30 minutes before n.c. 10 has no apparent impact on segmentation gene expression (Figures
295 S4B8-S4G8), corroborating previous results (Figure 3) indicating that Bcd-dependent
296 transcription in this time window is dispensable for embryonic viability.
297
298 The reliance of the most anterior gap gene expression (Kni1, Gt1, and Otd) on persistent Bcd-
299 dependent transcription may explain our previous observations that inhibiting Bcd

300 transcriptional activity both at very late or early stages impairs the proper formation of the
301 anterior-most segments (Figures 3C, 3J and 4C). Any short interruption of Bcd
302 transcriptional activity (from n.c. 10 till the very end of n.c. 14) abolishes the activation or
303 maintenance of gap gene expression domains. As they lie on top of the hierarchical gene
304 network defining cell fates, their loss alters cell fate decisions and leads to morphological
305 defects. Comparatively, the expression of gap gene domains at posterior positions is less
306 susceptible to perturbations in Bcd function. Consequently, cells arising from these domains
307 still commit to correct fates under Bcd deprivation at early or late stages, as reflected in Hox
308 gene expression patterns. We summarize this spatio-temporally coordinated Bcd
309 interpretation in Figure 6E. The more anterior structures, which have cell fates governed by
310 high Bcd concentration, require Bcd for an extended period of time. On the contrary, cells at
311 positions responding to low Bcd require a markedly shorter time window of exposure to Bcd
312 activity to commit to cell fates appropriate for their spatial position.

313 **Discussion**

314

315 **Optogenetic manipulation of transcription activity *in vivo***

316 Several recent studies have used elegantly designed optogenetic systems to unveil the
317 temporal role of signalling pathways in embryonic cell fate induction (Johnson et al., 2017;
318 Sako et al., 2016). As a common strategy, an ubiquitously expressed construct is utilized to
319 activate the upstream components of the signalling pathway in a light-responsive manner. In
320 this study, we developed and characterized an optogenetic tool to temporally switch on and
321 off of the transcriptional activity of the morphogen protein Bcd. In contrast to the previous
322 approaches, our light-sensitive protein CRY2::mCh::Bcd is present in the spatial distribution
323 of a native Bcd gradient. While the protein remains transcriptionally active in the dark, blue-
324 light induced conformational change of N-terminal CRY2 abolishes all direct target gene
325 expressions instantaneously. As such conformational change does not affect the DNA
326 binding specificities (Figures 2F-2G) or the spatial localization of the protein (Figure 1O), we
327 conclude that the inhibitory effect results from failure of transcriptional machinery assembly
328 due to conformational hindrance. It remains unclear whether such hindrance is caused by the
329 CRY2 conformational change alone or the effects of light-induced CRY2 oligomerization. It
330 will be of general interest to further explore if the N-terminal CRY2 exerts transcriptional
331 inhibition when tagged with other transcription factors, so that our optogenetic approach can
332 be more widely applied to understand the temporal readout of spatially distributed
333 transcription factors.

334

335 **The temporal pattern of Bcd signal integration is spatially inhomogeneous**

336 The continuous transitions between cell states in a developing embryo are governed by both
337 the transcriptional landscape and the transcriptional history of the cells. Therefore, not only

338 the local concentrations of the combinatorial transcription factors but also the timing and
339 duration of their presence are essential for the correct cell fate decisions. Bcd in the early fruit
340 fly embryo provides the very initial positional cues along the antero-posterior axis,
341 differentiating cells spanning ~10 embryonic segments (Driever et al., 1989). The gradient
342 profile of Bcd is highly dynamic throughout the blastoderm stage, with no clear steady-state
343 (Little et al., 2011). Such dynamics make the temporal aspects of Bcd interpretation critical
344 for precise decoding of the morphogen. A previous study quantified the temporal evolution of
345 Bcd dosage at several gap gene expression boundaries, and deduced that the absolute Bcd
346 concentration is read out during early n.c. 14 (Liu et al., 2013). In comparison data-driven
347 models propose a much wider time window for Bcd readout, as decoding the gradient earlier
348 in development (Bergmann et al., 2007) or during its degradation in n.c. 14 (Verd et al.,
349 2017) gives rise to more accurate predictions of gap gene expression patterns. Direct testing
350 of these ideas has previously been difficult due to a lack of temporal manipulation of Bcd
351 activity.
352
353 Consistent with previous studies, we find that the time window ranging from n.c. 13 to early
354 n.c. 14 is indeed most critical for Bcd-dependent patterning of downstream genes;
355 deprivation of Bcd transcriptional activity during this period leads to severe patterning
356 defects in all the Bcd-dependent embryonic regions, from the most anterior to mesothoracic
357 segment (Figures 3F-3G). On the other hand, Bcd activity in this critical time window is
358 sufficient for the proper cell fate induction in mesothorax, regardless of Bcd activity in rest of
359 the time points throughout the blastoderm stage. Further, the more anterior the cells locate,
360 the wider time window of Bcd activity is required (Figure 3), as in the extreme case, the
361 proper formation of the most 'needy' clypeolabrum segment, patterned by the highest Bcd

concentration, requires Bcd-dependent transcription from n.c. 10 to the very end of n.c. 14 (Figures 4B-4C).

Similar correlations between morphogen concentration and required duration have been observed in Shh patterning of the vertebrate neural tube (Dessaud et al., 2007). Shh signalling is temporally integrated by a genetic feedback loop that leads to desensitization of cells to Shh signal over time. In this way, the duration of Shh input is translated into differential gene expression. Considering the rapid establishment Bcd target gene expression patterns, it is unlikely that the same mechanism is utilized here. Our quantitative analysis on gap gene expression stand in line with two alternative mechanisms underlying such temporal integration: (1) The anterior gap genes have slower transcription rates than the posterior gap genes, therefore they require Bcd for longer duration. A recent study has proposed a role of transcription kinetics in shaping the timing as well as the spatial range of morphogen response (Dubrulle et al., 2015). Here, we find that the mRNA production and protein turnover of the anterior gap genes are in a tight balance. Once this balance is tipped by inhibiting transcription even for a short period of time, the protein expression can no longer be maintained (Figure. 6A-6D). In contrast, inhibiting the transcription of more posterior genes, such as hb, in mid to late n.c. 14 does not affect their expression, potentially due to an excessive mRNA pool. (2) Bcd-dependent transcription serves as a priming role in early stages for proper expression of anterior gap genes. Restoring native Bcd dosage in later stages fails to initiate *bona fide* gene expression in the very anterior domains, suggesting that cells are no longer competent to adopt anterior-most cell fates. Whether Bcd primes cell competency by chromosomal remodeling to increase accessibility (Blythe and Wieschaus, 2016) or inhibiting the otherwise ectopically expressed repressive factors must be subjected to further investigation.

387 **Temporal interpretation ensures developmental precision by buffering noises**

388 What role does temporal coordination of morphogen interpretation play in achieving precise
389 cell fate determination? In *Drosophila* - as in all long germband insects - the embryonic
390 segments emerge simultaneously (Sander, 1976). Bcd-dependent cell fate specification
391 appears to move from posterior towards the anterior in a sequential manner. The most
392 posterior cells "lock-in" to their correct fate decisions by early cycle 14, becoming refractory
393 to further alterations of Bcd dosage. Meanwhile, more anterior genes remain sensitive to Bcd
394 dosage for much longer periods. Therefore, this mode of temporal interpretation can cope
395 better with a temporally dynamic morphogen gradient or fluctuations in local concentration.
396 This temporal sequence of boundary determination may help to assure robustness of gene
397 boundary specification within such a short developmental time.

398

399 **Tight coupling between transcription and morphogenesis**

400 Our optogenetic transcriptional manipulation approach brings further insights into how
401 transcription is tightly coupled to cell specification and could be extrapolated to other
402 analyses as morphological movements during embryogenesis. For example, we find that Bcd-
403 dependent transcription not only determines the position of cephalic furrow invagination
404 (Vincent et al., 1997) but also dictates the timing of when this tissue remodeling occurs
405 (Figure S5). Finally, coupling optogenetic manipulations with light-sheet microscopy, we can
406 spatially restrain transcriptional inhibition to one lateral side of the embryo. This locally
407 alters cell fates, resulting in morphological defects – such as in cephalic furrow formation -
408 while the contralateral side remains intact (Movie S2). Spatio-temporal manipulation of Bcd
409 activity in the early embryo is thus an exciting avenue for future study.

410

Acknowledgments

We thank Eric Wieschaus, Thomas Gregor, Johannes Jaeger, Tiffany Cook, Thomas C. Kaufman and James Sharpe for sharing precious reagents. We acknowledge Eric Wieschaus, Enrique Martin-Blanco, James Briscoe, Philip Ingham, Shelby Blythe and all Saunders' lab members for fruitful discussions. This work was supported by the National Research Foundation Singapore under an NRF Fellowship to T.E.S. (NRF2012NRF-NRFF001-094).

Author Contributions

A.H., C.A. and T.E.S. designed the study. A.H. and C.A. performed the experiments, S.Z. performed the computational analysis and N. S. T. created the Bcd MiMIC mutant. A.H., C.A. and T.E.S. wrote the manuscript. All authors participated in the final version of the manuscript.

The authors declare no competing financial interest.

423 **MATERIALS AND METHODS**

424 **Fly stocks and genetics**. A CRY2::mCh::Bcd fusion construct was generated by replacing
425 the eGFP sequence in the P[*egfp-bcd*] vector(Gregor et al., 2007a) by the CRY2::mCherry
426 sequence. The original vector was digested with NheI and SphI to remove eGFP and the
427 CRY2::mCherry sequence was amplified by PCR from the AddGene plasmid #26866
428 (Kennedy et al., 2010) using primers appended with NheI and SphI restriction sites. The
429 resulting **P[*cry2-mcherry-bcd*]** construct contained *bcd* natural 5' and 3' UTRs as well as
430 upstream enhancers. P-element transformation was carried out by BestGene Inc. and seven
431 transgenic lines on the 3rd chromosome were recovered. Two different lines expressing
432 CRY2::mCh::Bcd respectively at low (CRY2^{low}) and high (CRY2^{high}) levels (mCherry
433 fluorescent intensity) were employed throughout our analyses. Transcription and mRNA
434 localization in the transformed flies was expected to recapitulate those of endogenous *bcd*.

435 A *bcd* knockout fly line was generated by CRISPR-mediated insertion of a MiMIC cassette
436 (Venken et al., 2011) (injection performed by GenetiVision). The progenies from
437 homozygous females phenocopied *bcd*^{E1} developmental defects(Frohnhöfer and Nüsslein-
438 Volhard, 1986). The CRY2::mCh::Bcd (CRY2^{high}) transgenic was recombined with the *bcd*
439 knockout allele to establish a stable line. All experiments were carried out with this fly line
440 unless otherwise stated.

441 Additionally, the fly line nanos>Gap43::mCh (Martin et al., 2010) was used for light-sheet
442 imaging.

443 **Temporally patterned illumination.** Duration of syncytial nuclear cycles were evaluated by
444 imaging embryos on a bright-field stereomicroscope at 25 °C. The blastoderm stage (from
445 fertilization to the onset of gastrulation) spans 2.5 hours. The last syncytial cycle (n.c. 14),
446 demarcated by the last division wave and the first sign of gastrulation, lasts about 45 minutes.
447 The penultimate cycle (n.c. 13) lasts 15 minutes, while the duration of the previous three
448 cycles (n.c. 10-12) is about 30 minutes in total. To maintain dark condition, embryos were
449 observed or imaged with all light sources covered by amber paper (*i.e.* blocking blue light).
450 To induce the conformational change of the CRY2 protein, we illuminated the embryos on a
451 Nikon LED light base at 488 nm wavelength. The light intensity was measured with an
452 intensity power meter. All experiments were carried out at 4.0 mW unless otherwise stated.
453 For temporally patterned illumination, blastoderm stage embryos were selected in the dark
454 condition and exposed to light. The illumination treatment of each embryo was recorded. The
455 illumination duration was timed from the moment of light exposure until the onset of
456 gastrulation. When the illumination treatment was followed by dark recovery, we continued
457 the timing by observing embryos with a light source covered with amber paper until
458 gastrulation initiated.

459 **Immunostaining.** Embryos at the desired stages were dechorionated by household bleach
460 and fixed in heptane saturated by 37 % paraformaldehyde (PFA) for 1 hour. The vitelline
461 membrane was subsequently manually removed. Prior to incubation with primary antibodies,
462 embryos were blocked with 10% BSA in PBS. Image-iT®FX signal enhancer was used as
463 blocking reagent instead of 10% BSA for Cad staining. Antibodies used were rabbit anti-
464 mCherry (1:100, AbCam), rat anti-Caudal (1:100), guinea pig anti-Hb (1:2000), rabbit anti-
465 Gt (1:800), guinea pig anti-Kr (1:800), guinea pig anti-Kni (1:800), guinea pig anti-Eve
466 (1:800), guinea pig anti-Otd (1:800), mouse anti En (1:100, DSHB), rabbit anti-Dfd (1:100),
467 mouse anti-Scr (1:10, DSHB), mouse anti-Antp (1:10, DSHB), mouse anti-Ubx (1:100,

468 DSHB) and mouse anti-Abd-B (1:100, DSHB). Primary antibodies were detected with Alexa
469 Fluor-labelled secondary antibodies (1:500; LifeTech). Embryos were co-stained with
470 Phalloidin conjugated with Alexa Fluor for staging purpose. Embryos were mounted in
471 AquaMount (PolySciences, Inc.) and imaged on a Zeiss LSM710 microscope with a C-
472 Apochromat 40x/1.2 NA water-immersion objective. Cad antibody was kindly provided by
473 Eric Wieschaus. Hb, Gt, Kr, Kni and Eve antibodies were gifts from Johannes Jaeger. Otd
474 was kindly given by Tiffany Cook. Last, Dfd antibody was a gift from Thomas C. Kaufman.

475 **Gradient quantification.** Images were projected using a maximum intensity projection and
476 then nuclei segmented using Ilastik (Sommer et al., 2011). Nuclei were binned into 5mm
477 spatial steps along the anterior-posterior axis using Matlab. Bcd nuclear intensity plots were
478 created after background subtraction using morphological opening. Profiles fitted as
479 described in Liu (et al., 2013).

480 **Live imaging and quantification of MS2 RNA reporter.** Embryos were collected,
481 dechorionated and mounted on a MatTek dish under dark condition. The embryos were
482 imaged on a custom-built Spinning Disc microscope with a Nikon Apo 40X/1.25 water-
483 immersion objective. The pixel size is 409 nm and the image resolution is 1024x1024 pixels.
484 At each time point a stack of 35 images separated by 3 µm was acquired. The temporal
485 resolution was 40 seconds. Each Z-stack for each time point was Z-projected (maximum
486 intensity) prior to subsequent quantification. The workflow to analyze MS2 spots goes as
487 follow: we extracted the boundary of the embryo to exclude false positive, we applied a
488 threshold and regional intensity comparison to locate all MS2 spots and we tracked these
489 spots using a minimal distance criterion. To refine our analysis, we considered spot tracks
490 lasting for a minimum of 4 time frames. We plotted the probability distribution of MS2 spots
491 persistence into 2 regions, *i.e.* the anterior and posterior domains (Fig. 2e and d). Further, we
492 subdivided the anterior *hb* domain into five distinct regions along the AP axis, *i.e.,* 100-75,
493 75-70, 70-65, 65-60 and 60-40 %EL. We plotted the probability distribution of MS2 spots
494 persistence in these regions and in the posterior *hb* domain (Extended data Fig 1c and d).
495 MS2 quantification is further described in the Supplementary Materials 1.

496 **Chromatin immunoprecipitation and qPCR.** Late n.c. 14 embryos aged in the dark or
497 exposed to light (at 4mW) for 45 minutes were dechorionated in household bleach. Embryos
498 were crosslinked for 15 minutes in a solution containing 2 ml of PBS, 6 ml of Heptane and
499 180 µl of 20% paraformaldehyde. Embryos were transferred to a 1.5 ml tube and the
500 crosslinking was quenched with the addition of 125 mM glycine in PBS 15 min after the start
501 of fixation. ChIP samples were essentially prepared as described in Blythe and Wieschaus,
502 2015(Blythe and Wieschaus, 2015). Sonication was performed on a Sartorius stedim
503 Labsonic® M with a microtip horn. An input control corresponding to 2% of the volume per
504 reaction was taken after sonication. Immunoprecipatations (IPs) were performed with a
505 mCherry antibody (Clonetech #632496) for 15 hours at 4ºC. ChIPped DNA were extracted
506 with a Qiaquick spin column (Qiagen). Real-time quantitative PCR was performed using
507 SYBR® Green Assay (Thermo Fisher Scientific) on a Bio-Rad CFX96 Real-time system.
508 Four primer pairs were used, respectively probing Hb (P2 enhancer), Gt, Otd and Kr.
509 Additionality, a primer pair was designed 1kb downstream of the P2 enhancer (HbP2+1kb) to
510 be used as a negative control. The percent input method (100*2^(Adjusted input – Ct(IP))
511 was used to normalize ChIP-qPCR data. Further, the relative %Input for illuminated embryos
512 was calculated as compared to the embryos in dark and summarized in a bar chart. In the case
513 of the HbP2+1kb, data were compared to HbP2 results. Three independent replicates have
514 been performed for each primer sets and the significance was calculated with a standard t-test.

515 **Cuticle preparation.** Embryos subjected to temporally patterned illumination were allowed
516 to develop until the end of embryogenesis. The embryos were then dechorionated and
517 incubated into a mixture of Hoyer's medium and Lactic acid in a 1:1 ratio at 65 °C between
518 an imaging slide and a cover slip. For an exhaustive description of the method used see
519 Alexandre (2008).

520 **Gap gene profile quantification.** Confocal Z-stack images were Z-projected (maximum
521 intensity) in Fiji for further analysis. Images were rotated to orient embryos anterior left and
522 dorsal up and rescaled to same embryo length and width. Intensity profiles along the antero-
523 posterior axis were measured in Fiji. For Hb, the intensity profile was normalized to the peak
524 value of the posterior domain. To determine the boundary positions of Kr and Kni expression
525 domains, we plotted the intensity profiles along the AP axis and defined the boundary at the
526 position with intensity equals to half of the peak value.

527 **Hemi embryo illumination on a Light-Sheet microscope.** Embryos were dechorionated as
528 described earlier and mounted in 1% agarose on a Fluorinated ethylenepropylene (FEP)
529 capillary (TEF-CAP, #AWG18LW-FEP). Embryos were then imaged on a custom-built
530 Light-Sheet Microscope with a Nikon Apo 1 WD 25X/1.10 water-dipping objective.
531 Embryos expressing CRY2::mCh::Bcd and the membrane marker Gap43::mCh were
532 recorded using a 561nm excitation laser. The pixel size was 510 nm and the image resolution
533 was 1024x1024 pixels. At each time point a stack of 100 images separated by 2.5 µm was
534 acquired. The temporal resolution was 30 seconds. This illumination setup mimics dark
535 condition as no morphological defects were observed. To stimulate CRY2 conformational
536 change in just one half of the embryo, a region on one lateral side of the embryo was defined
537 from the most apical section up to 70 µm down. A stack of 100 sections separated by 0.7 µm
538 were illuminated. The illumination was carried out from the beginning of the n.c. 14 (5 min
539 after the establishment of the cellularization furrow) for 20 min with a 488 nm laser.
540 Following illumination, embryos were imaged solely with the 561 nm excitation laser.

541 **FIGURES**

542

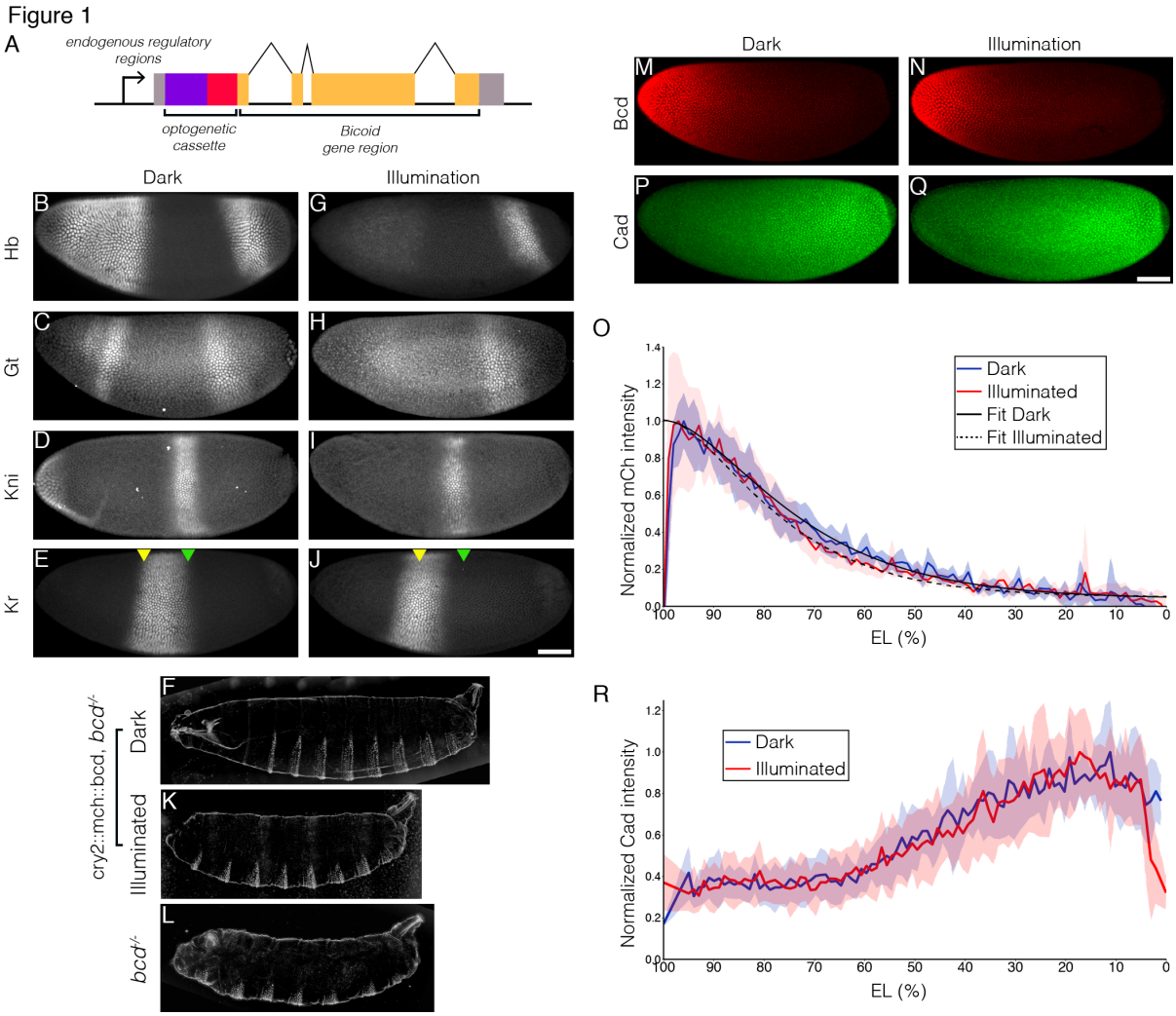

543
544

545 **Figure 1. Optogenetic tool to manipulate Bcd-dependent transcription activity**
546 (A) Schematic illustration of CRY2::mCh::Bcd construct; CRY2 optogenetic cassette tagged with
547 mCherry fluorescent protein is fused to the N-terminal of Bcd coding sequence; expression of the
548 construct is under the regulation of the endogenous *bcd* regulatory sequence. (B-J) Embryos having
549 developed in the dark (B-E) or light (G-J) fixed at the end of the blastoderm stage and stained for Hb
550 (B and G), Gt (C and H), Kni (D and I) and Kr (E and J). Yellow and green arrowheads indicate,
551 respectively, the position of the anterior and posterior boundaries in the dark. (F,K and L) Cuticle
552 patterns of embryos with maternally loaded *cry2::mch::bcd* having developed in the dark (F) or light
553 (K) in the first 2.5 h AEL as compared to (L) $bcd^{-/-}$ embryos. (M, N, P and Q) Embryos in the dark (M
554 and P) or light (N and Q) stained for mCh (M and N) and Cad (P and Q) at early n.c. 14.(O and R)
555 Average nuclear intensity of CRY2::mCh::Bcd (O) or Cad (R) normalized to peak value is plotted vs.
556 AP position (% EL) in dark (blue curve) and light (red curve). (O) Data were fitted to an exponential
557 curve shown by smooth lines with length scales around 80 µm. Shaded error bars are across all nuclei
558 of all embryos at a given position. n = 5-7 embryos per condition. Scale bar, 50µm.

Figure 2

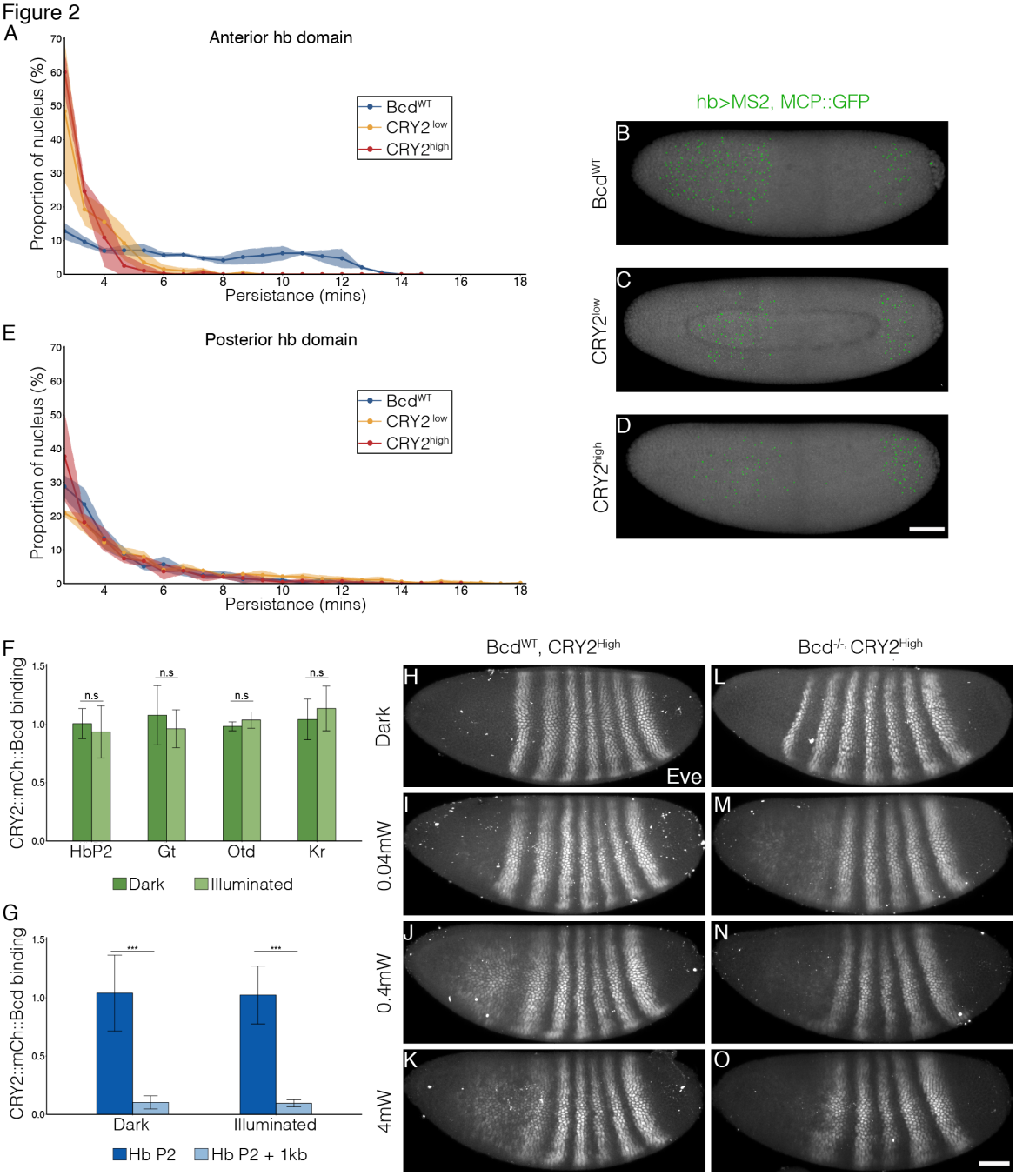

Figure 2. Inhibitory effect on Bcd-dependent transcription is gene-dosage and light-power dependent

(A and E) Proportion of the nuclei positive for *hb* transcription plotted vs. the persistence of transcription activity during n.c. 13 in control (blue), CRY2^{low} (orange) and CRY2^{high} (red) embryos of *hb* anterior (A) and posterior (E) domain. n = 3 embryos per genotype. (B-D) Snapshots of embryos expressing hb>MS2, MCP::GFP in n.c.13. Embryos are maternally loaded with only endogenous *bcd* (B), or together with *cry2::mch::bcd* at low(C) or high (D) level. MCP::GFP signals are tracked and marked with green dots. (F and G) Chromatin immunoprecipitation quantitative PCR (ChIP-qPCR) characterization of CRY2::mCh::Bcd binding to Hb (P2 enhancer), Gt, Otd and Kr in the light for 45 mins (4mW) as compared to embryos aged in the dark (F) and to 1kb downstream of the Hb P2 enhancer in the dark and light conditions (G). (H-O) Eve staining in embryos maternally loaded with cry2::mch::bcd in bcd^{WT} (H-K) or *bcd* null (L-O) background; embryos have developed in dark (H and L) or illuminated with blue light at 0.04mW (I and M), 0.4mW (J and M) or 4mW (K and O). Scale bar, 50µm.

Figure 3

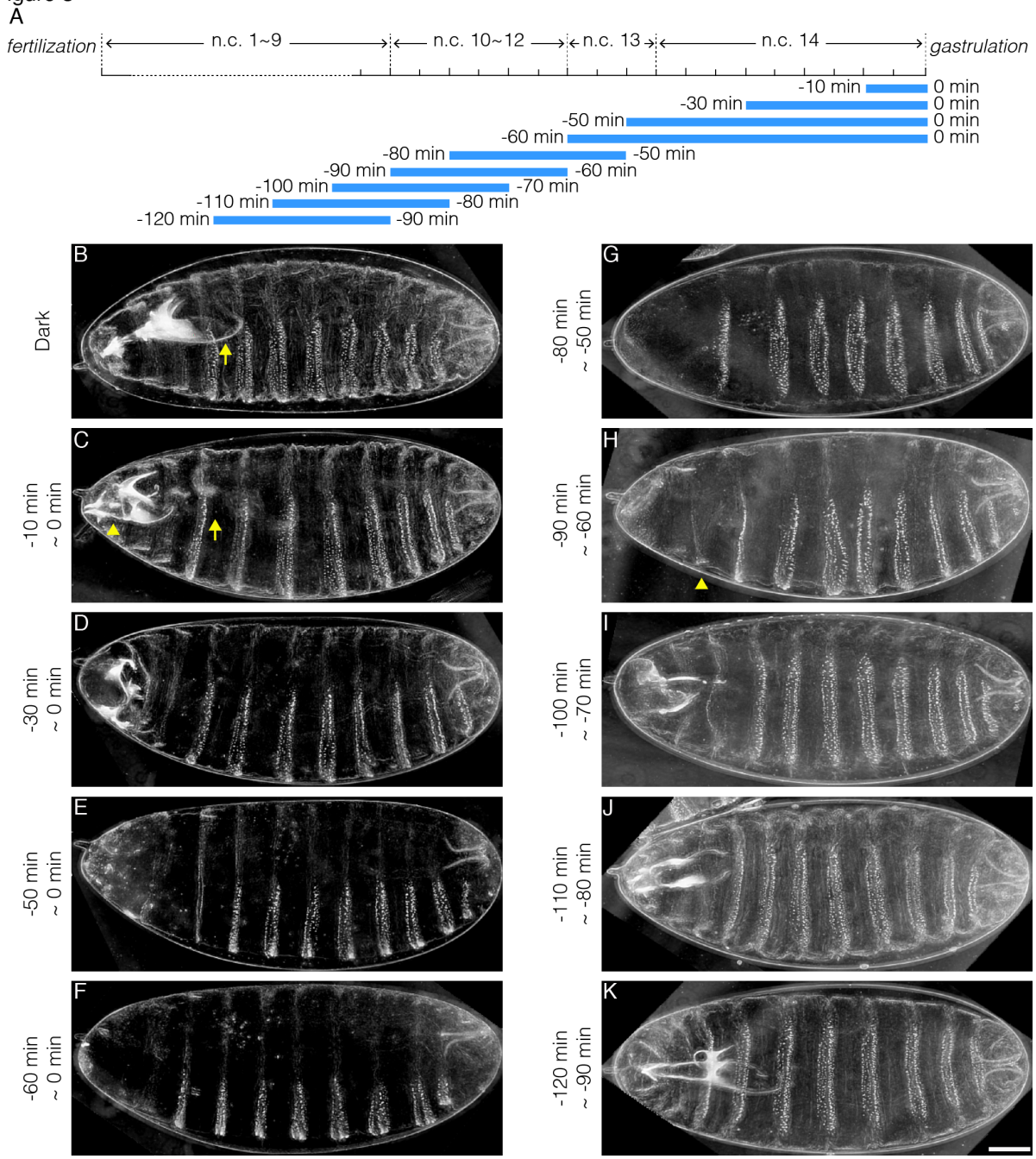

Figure 3. Illumination across different time windows causes embryonic lethality with varied severity

(A) Schematic demonstration of illumination time windows. Blue bars indicate illumination while the absence of blue bars indicates dark condition. The onset of gastrulation is defined as time 0. Negative values refer to specific time before gastrulation. The start and the end of illumination is indicated by the number on the left and right side of the blue bars, respectively. (B-K) Cuticle preparation of embryos illuminated in different time windows. The illumination time is indicated on the left of each image. (B) Arrow, pharynx wall; (C) Arrow, absence of pharynx wall. Arrowhead, missing structures lying between mouth hooks and cephalo-pharyngeal plates. (K) Arrowhead, denticle belt of thorax segment. Scale bar, 50μm.

Figure 4

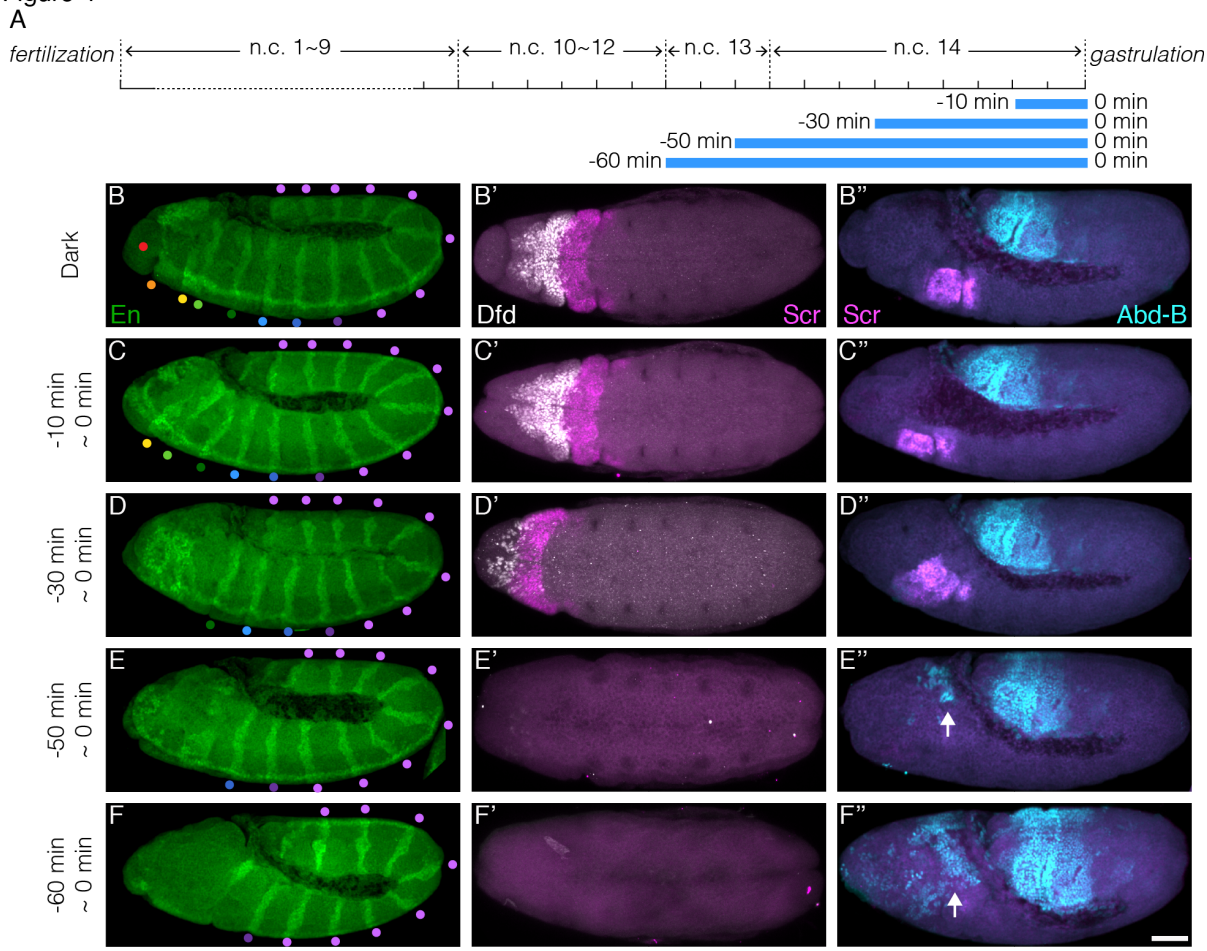

Figure 4. Illumination at the end of blastoderm stage causes wrong cell fate determination in anterior embryonic segments

(A) Schematic demonstration of illumination time windows at the end of blastoderm stage. Illumination starts at certain time before gastrulation and ends at the onset of gastrulation as indicated by blue bars. (B-F, B'-F' and B''-F'') Embryos illuminated in different time windows as indicated at the left side of each panel are fixed by the end of GBE and stained for En (B-F), Deformed (Dfd, white) and Scr (magenta) (B'-F'), Scr (magenta) and Abd-B (cyan)(B''-F''); (B-F) Colored dots represent embryonic segments. Red, clypeolabrum; orange, stomodeum; yellow, mandibular lobe; light green, maxillary lobe; dark green, labial lobe; light blue, prothorax; dark blue, mesothorax; dark purple, metathorax; and light purple, abdominal segments. (E'' and F'') Arrows, ectopic Abd-B expression. Scale bar, 50μm.

Figure 5

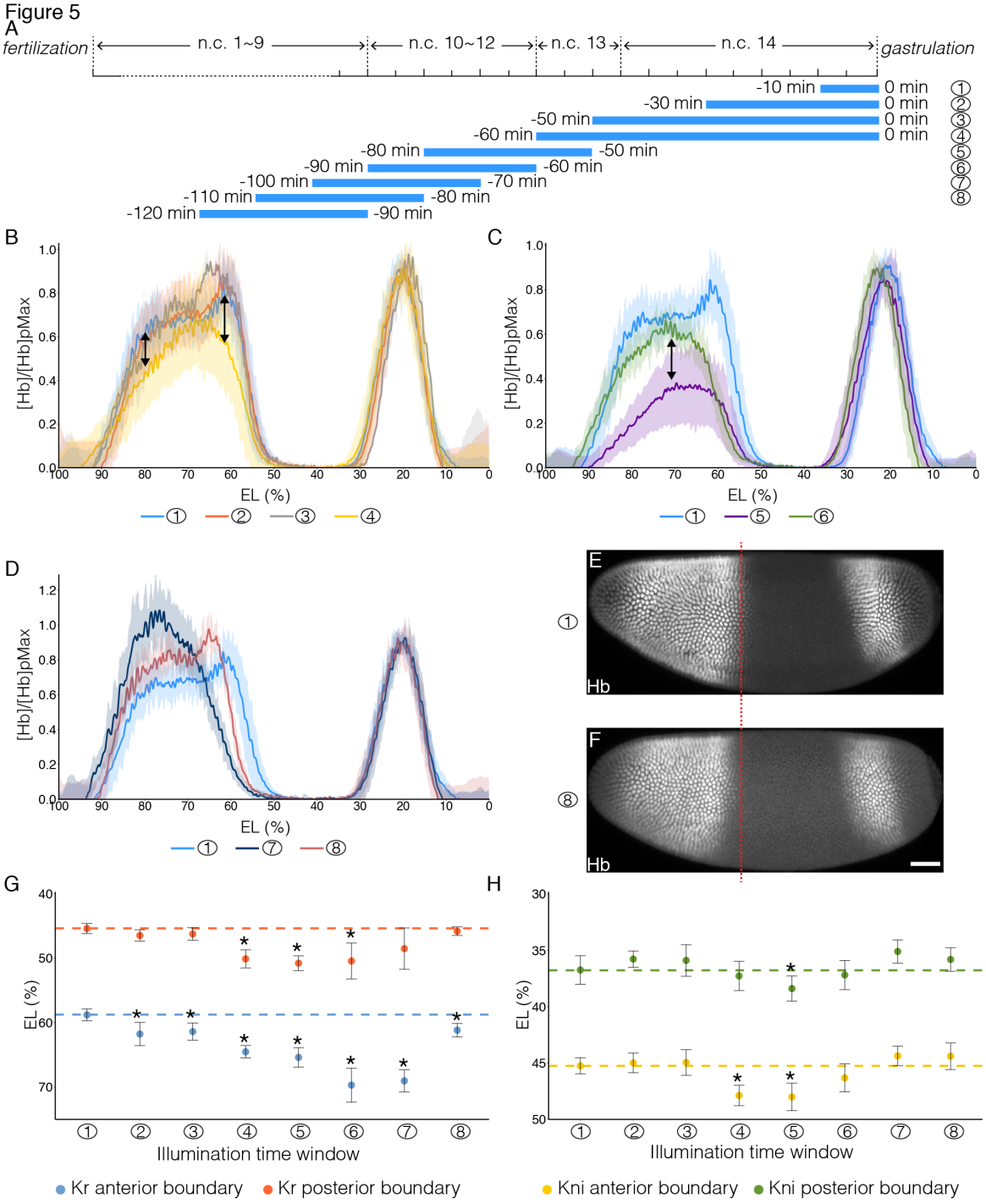

Figure 5. Impact of temporally patterned illumination on downstream gene expression
(A) Schematic demonstration of eight different illumination time windows. (B-D) Average Hb intensity normalized to posterior peak values plotted vs. AP position (% EL) in embryos having developed in different temporally patterned illumination. Sample numbers correspond to time windows shown in (A). (B-C) Double-headed arrows point out the changed expression level of Hb. (E and F) Embryos having developed in dark (E) or illuminated for 30 minutes before n.c.11 (F) are stained for Hb. Red dashed line indicates the position of posterior border of anterior Hb domain of embryo in (e). Scale bar, 50µm. (G and H) Position of Kr anterior border (G, blue dots), Kr posterior border (G, red dots), Kni anterior border (H, yellow dots) and Kni posterior border (H, green dots) under different temporal illumination as indicated by sample numbers. Error bars indicate s.d.; t-test was used for the statistical evaluation with *p<0.05. A total number of 70, 53 and 59 embryos were analyzed for expression of Hb, Kr and Kni, respectively.

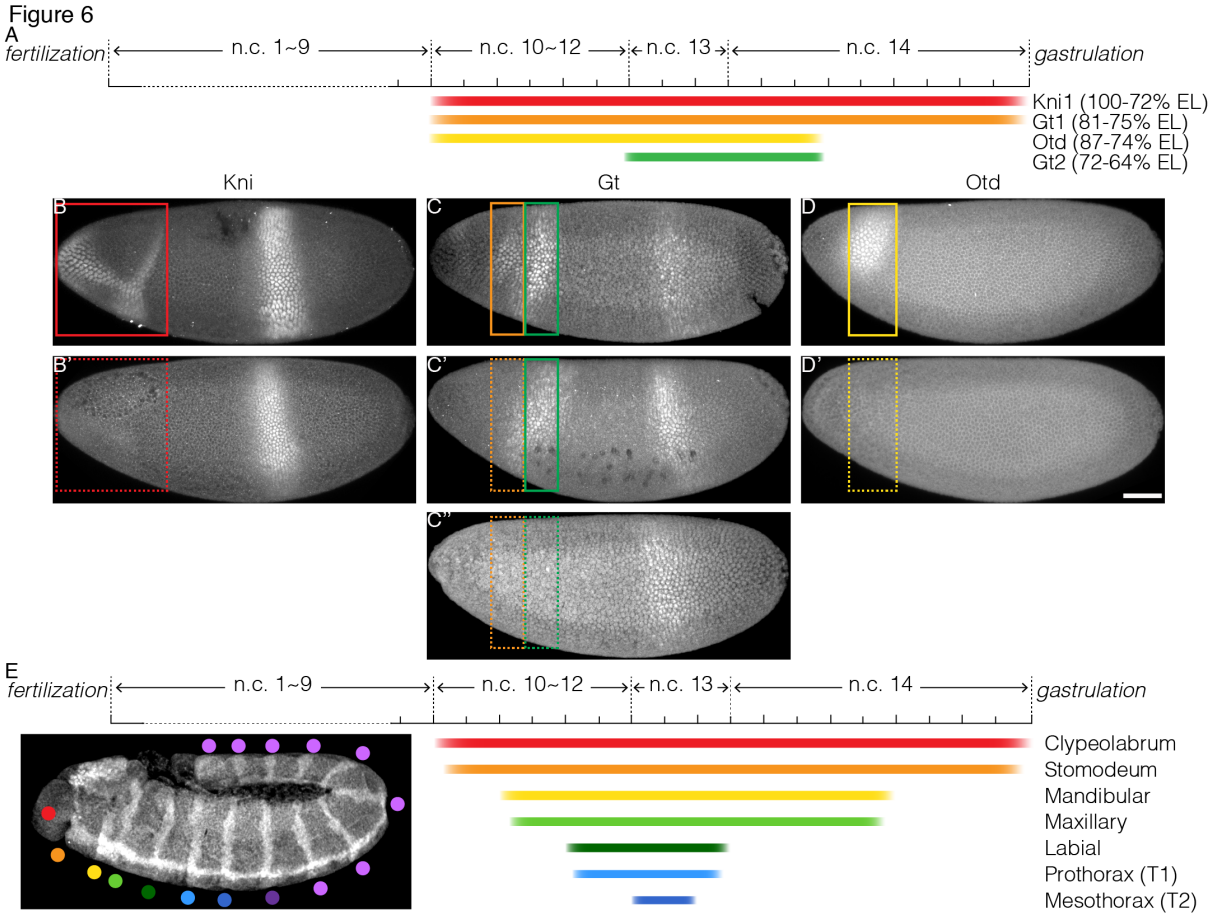

Figure 6. Temporal requirement of Bcd-dependent transcription for proper cell fate determination

(A) Schematic representation of required time windows of Bcd-dependent transcription for downstream gene expression; color bars indicate the time windows required for Bcd-dependent transcription to be on for correct expression of Kni1 (red), Gt1 (orange), Otd (yellow) and Gt2 (green); (B-D) embryos exhibiting the correct gene expression when Bcd-dependent transcription is active in required time window; colored boxes point out the corresponding expression domain; (B'-D' and C'') embryos showing defects in gene expression when Bcd-dependent transcription is interrupted in required time window; dashed boxes indicate failed expression. Scale bar 50µm. (E) Schematic diagram of temporal interpretation of Bcd morphogen. Colored bars indicate the time windows required for Bcd-dependent transcription for correct cell fate determination in different embryonic segments.

Figure S1

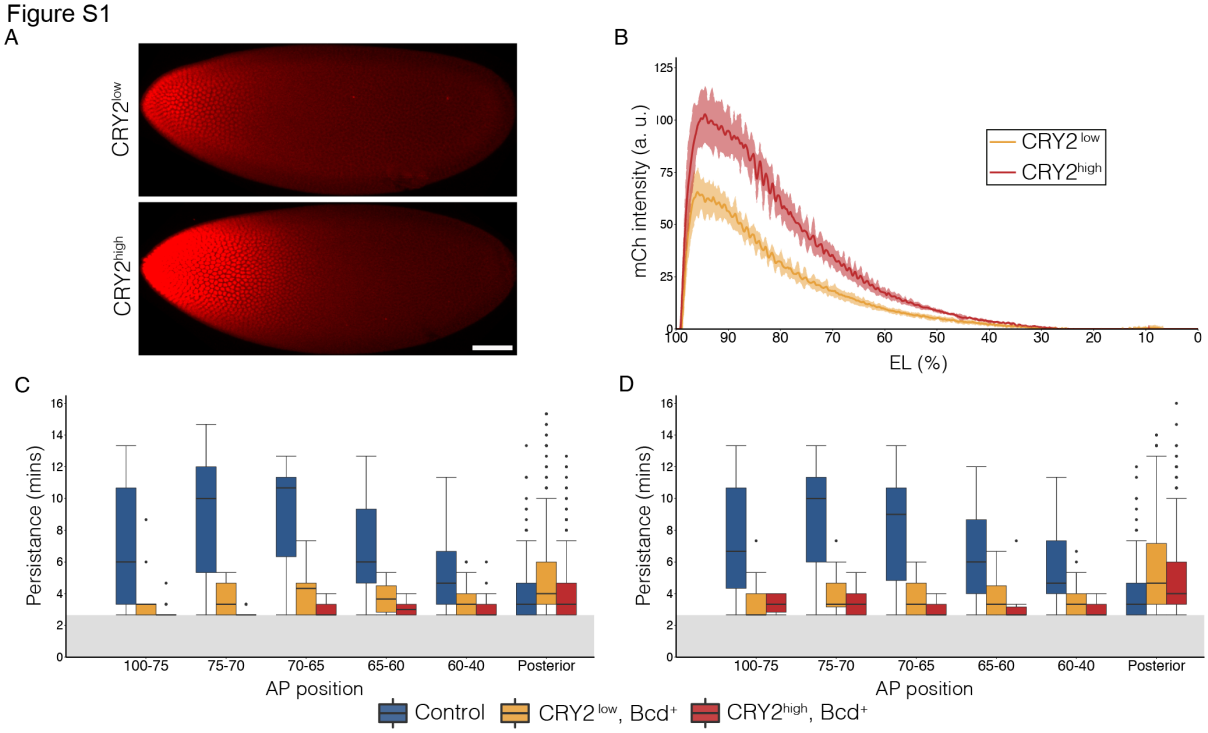

628
629
630 **Figure S1. Expression profiles in CRY2^{low} and CRY2^{high} embryos and effect of illumination on**
631 **hb mRNA production along the AP axis**
632 (A) Snapshots of embryos expressing CRY2::mCh::Bcd at comparatively low (top panel) and high
633 (bottom panel) level at late n.c. 14. Scale bar, 50 µm. (B) Average nuclear mCherry intensity in
634 CRY2^{low} (orange curve) and CRY2^{high} (red curve) embryos at late n.c. 14 is plotted vs AP position (%
635 EL). Shaded error bars are across all nuclei of all embryos at a given position. n = 8 embryos for
636 CRY2^{low} and n = 5 embryos for CRY2^{high}. (C and D) Box plot showing the persistence of *hb*>MS2
637 puncta in control (blue), CRY2^{low} (orange) and CRY2^{high} (red) embryos. Anterior *hb* domain is
638 subdivided into five distinct regions along AP axis, *i.e.,* 100-75, 75-70, 70-65, 65-60 and 60-40% EL.
639 Data is quantified in these regions as well as *hb* posterior domain, respectively. The cutoff value for
640 statistical analysis is 160s as shown by the grayed regions. Each box shows the counts for a single
641 embryo.

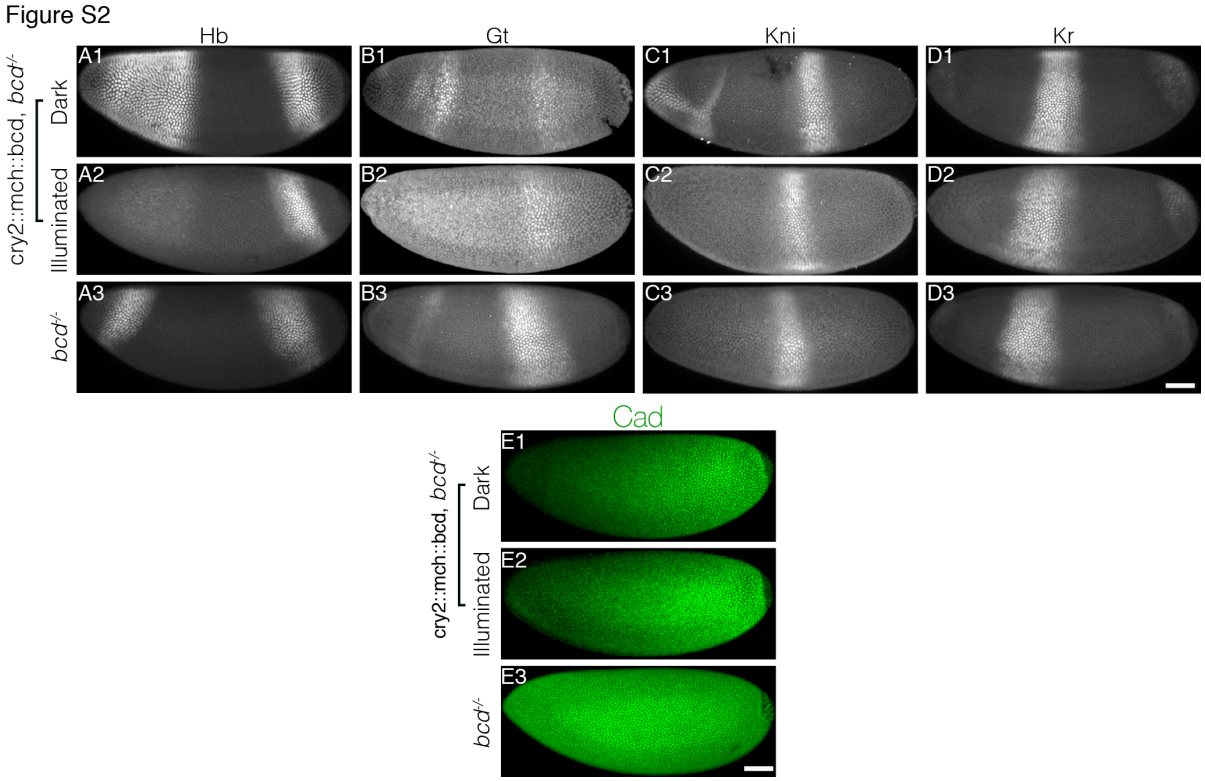

Figure S2. Comparison of gap gene and Caudal expression patterns between optogenetic and *bcd* mutant embryos

(A-E) Embryos laid by females expressing CRY2::mCh::Bcd in a *bcd* null background having developed in the dark (A1-E1) or light (A2-E2), or by females of *bcd* mutant (A3-E3) fixed at the end of blastoderm stage and stained for Hb (A1-A3), Gt (B1-B3), Kr (C1-C3) and Kni (D1-D3), or fixed at early n.c.14 and stained for Cad (E1-E3). Scale bar, 50 µm.

Figure S3

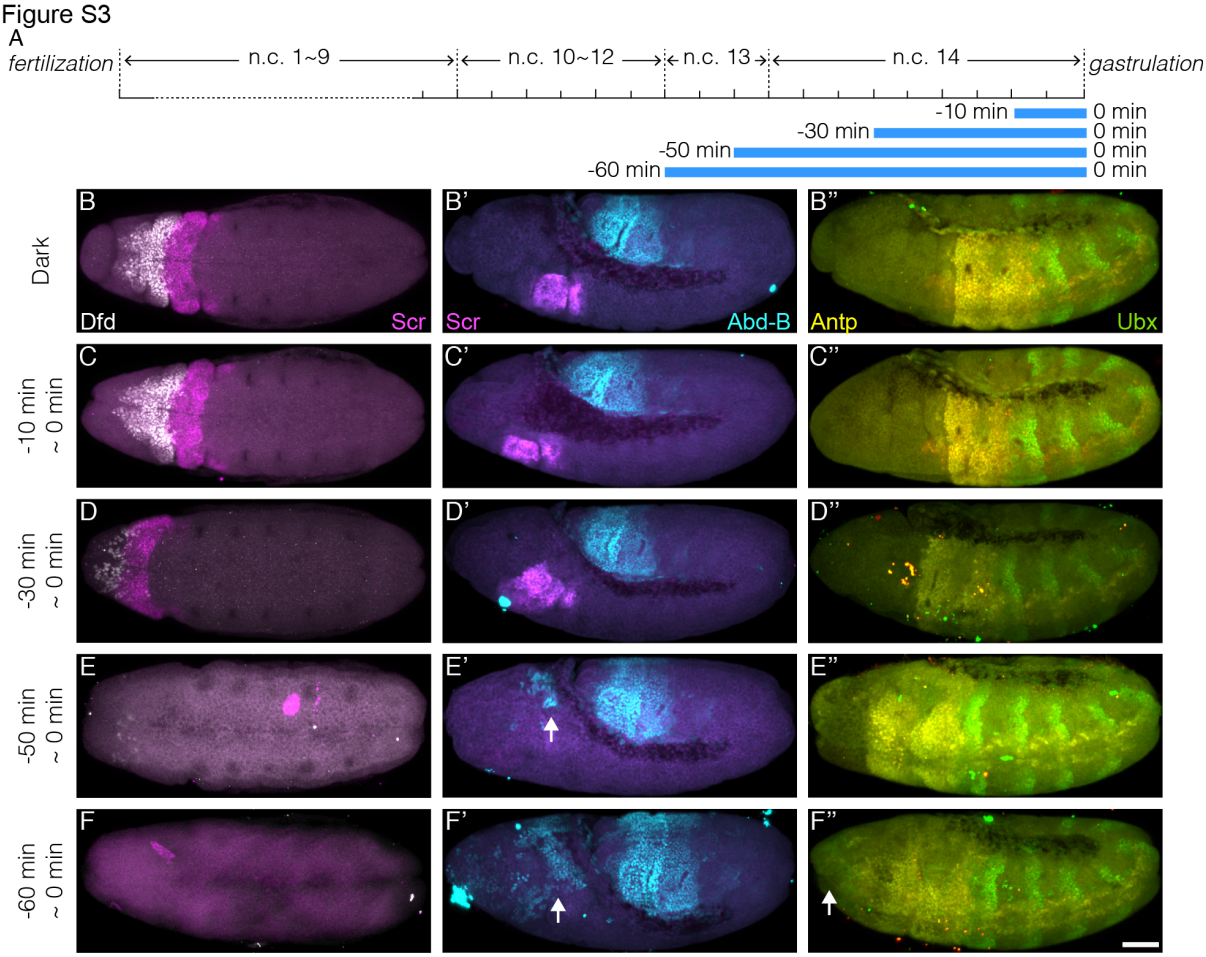

Figure S3. Hox genes expression pattern in increasing illumination time window

(A) Schematic demonstration of illumination time windows at the end of blastoderm stage. Illumination starts at certain time before gastrulation and ends at the onset of gastrulation as indicated by blue bars. (B-F, B'-F' and B''-F'') Embryos illuminated in different time windows as indicated on the left side of each panel are fixed by the end of GBE and stained for Dfd (white) and Scr (magenta) (B-F), Scr (magenta) and Abd-B (B'-F') and Antp (yellow) and Ubx (green)(B''-F''). Panels (B-F) and (B'-F') show the unprocessed images previously shown in Figure 4. (E' and F') Arrows, ectopic Abd-B expression. (F'') Arrow, ectopic Ubx expression. Scale bar, 50 µm.

Figure S4

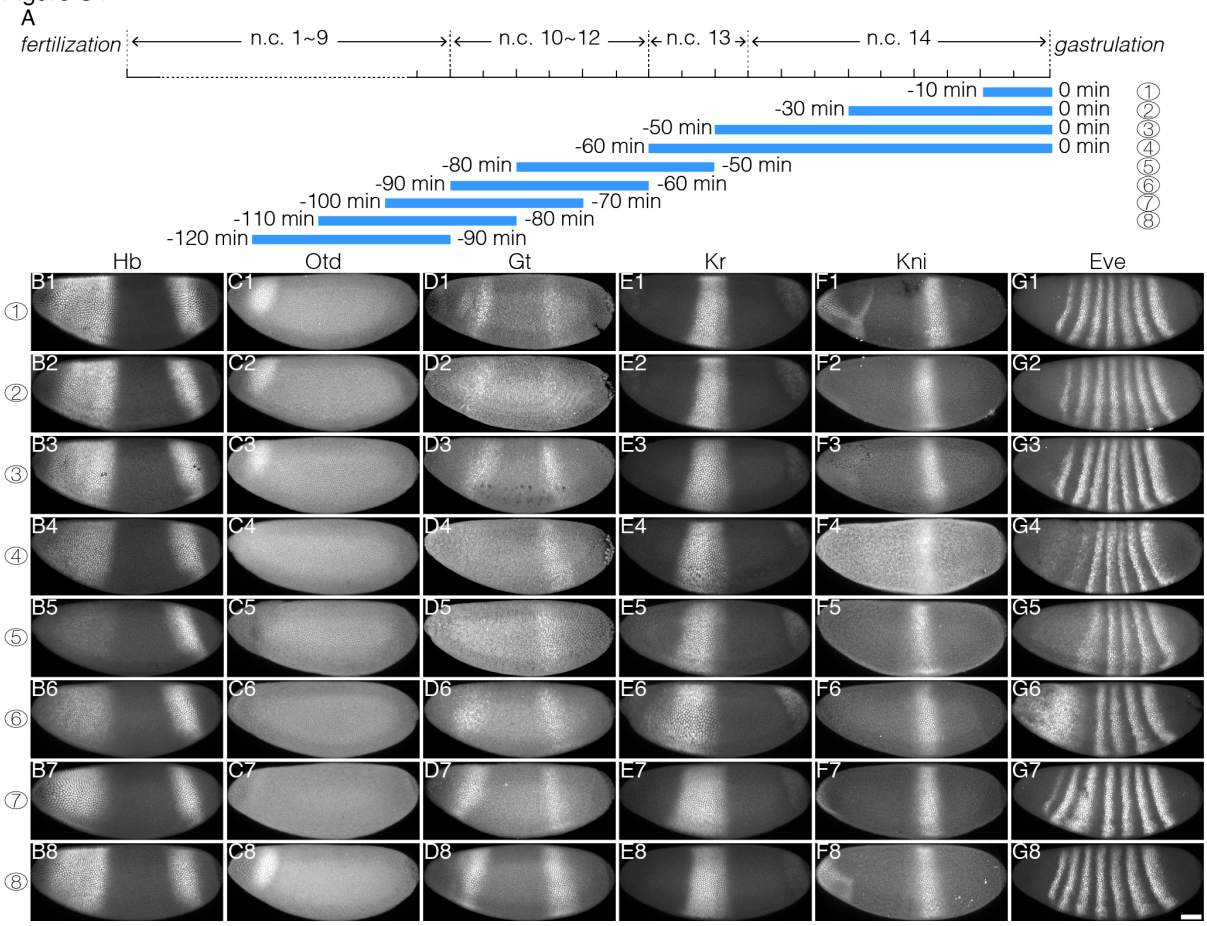

Figure S4. Impact of temporally patterned illumination on downstream gene expression
(A) Schematic demonstration of eight different illumination time windows. (B-G) Embryos illuminated in different time windows are fixed at the end of blastoderm stage and stained for Hb (B1-B8), Otd (C1-C8), Gt (D1-D8), Kr (E1-E8), Kni (F1-F8), and Eve (G1-G8); row 1-8 corresponds to 8 temporal illumination conditions shown in (A). Scale bar, 50 µm.

Figure S5

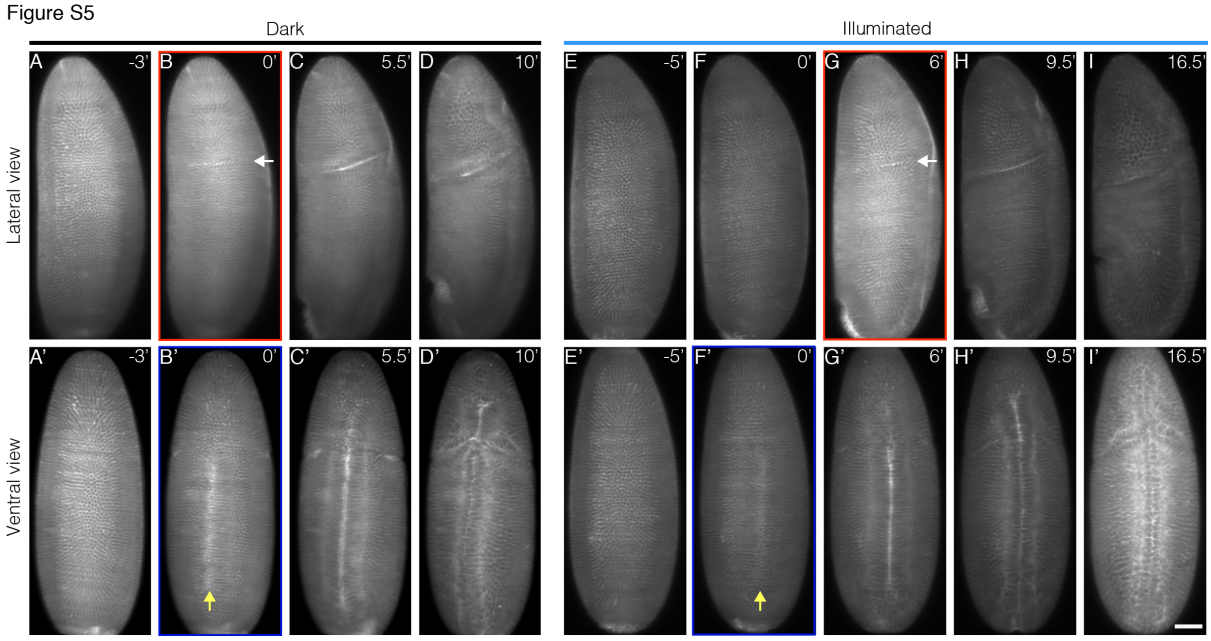

Figure S5. Impeding Bcd-dependent transcription during cycle 14 delays cephalic furrow invagination

Embryos expressing CRY2::mCh::Bcd and Gap43::mCh are imaged on a custom built light-sheet microscope. The embryos are illuminated with a 488nm laser for 20min starting 5min after the establishment of the cellularization furrow. Panels (A-D) and (A'-D') show respectively the lateral and ventral views for dark control embryos while (E-I) and (E'-I') show the lateral and ventral views for illuminated embryos. The red and blue rectangles indicate the time point marking the onset of cephalic furrow (white arrows) and ventral furrow (yellow arrows) invagination, respectively. Scale bar, 50 µm.

678 **Movie S1. CRY2::mCh::Bcd expression reduces the transcription activity of hb in the anterior**
679 **domain in blue light**
680 Embryos expressing the hb>MS2, MCP::GFP system were imaged throughout n.c. 13 and 14 with a
681 time resolution of 40s. Rows 1, 2 and 3 show respectively Control, $CRY2^{low}$ and $CRY2^{high}$ embryos.
682 The left column represents the raw data whilst the right column shows the segmented MS2 dots (in
683 green) as described in the Methods section.
684
685 **Movie S2. Bilateral cephalic furrow formation is uncoupled by single sided illumination**
686 Embryo expressing CRY2::mCh::Bcd and Gap43::mCh mounted on a custom-built Light-Sheet
687 microscope. The embryo was mounted during n.c. 13 and Gap43::mCh was used to follow its
688 developmental stage. Five minutes after the start of cellularization, one lateral side of the embryo was
689 illuminated for 20min, starting from its most apical section to 70µm deep (0.7µm interval). Whole
690 embryo recording (561nm laser) and hemi embryo illumination (488nm laser) were done
691 simultaneously with a time resolution of 30s. The top two panels show the lateral sides of the embryo,
692 the second panel being the illuminated one. The bottom two panels show the ventral and the dorsal,
693 respectively.

694 **REFERENCES**

695 Alexandre, C. (2008). Cuticle Preparation of Drosophila Embryos and Larvae. Methods Mol.
696 Biol. 197–205.

697 Ali-Murthy, Z., and Kornberg, T.B. (2016). Bicoid gradient formation and function in the
698 Drosophila pre-syncytial blastoderm. Elife *5*, 1–18.

699 Bergmann, S., Sandler, O., Sberro, H., Shnider, S., Schejter, E., Shilo, B.Z., and Barkai, N.
700 (2007). Pre-steady-state decoding of the bicoid morphogen gradient. PLoS Biol. *5*, 0232–
701 0242.

702 Blythe, S.A., and Wieschaus, E.F. (2015). Zygotic genome activation triggers the DNA
703 replication checkpoint at the midblastula transition. Cell *160*, 1169–1181.

704 Blythe, S.A., and Wieschaus, E.F. (2016). Establishment and maintenance of heritable
705 chromatin structure during early *Drosophila* embryogenesis. Elife *5*, e20148.

706 Dessaud, E., Yang, L.L., Hill, K., Cox, B., Ulloa, F., Ribeiro, A., Mynett, A., Novitch, B.G.,
707 and Briscoe, J. (2007). Interpretation of the sonic hedgehog morphogen gradient by a
708 temporal adaptation mechanism. Nature *450*, 717–720.

709 Dessaud, E., Ribes, V., Balaskas, N., Yang, L.L., Pierani, A., Kicheva, A., Novitch, B.G.,
710 Briscoe, J., and Sasai, N. (2010). Dynamic assignment and maintenance of positional identity
711 in the ventral neural tube by the morphogen sonic hedgehog. PLoS Biol. *8*.

712 Driever, W., Thoma, G., and Nusslein-Volhard, C. (1989). Determination of spatial domains
713 of zygotic gene expression in the Drosophila embryo by the affinity of binding sites for the
714 bicoid morphogen. Nature *340*, 363–367.

715 Dubrulle, J., Jordan, B.M., Akhmetova, L., Farrell, J.A., Kim, S.H., Solnica-Krezel, L., and
716 Schier, A.F. (2015). Response to Nodal morphogen gradient is determined by the kinetics of
717 target gene induction. Elife *4*, 1–27.

718 Frasch, M., and Levine, M. (1987). Complementary patterns of even-skipped and fushi tarazu
719 expression involve their differential regulation by a common set of segmentation genes in
720 Drosophila. Genes Dev. *1*, 981–995.

721 Frohnhöfer, H.G., and Nüsslein-Volhard, C. (1986). Organization of anterior pattern in the
722 Drosophila embryo by the maternal gene bicoid. Nature *324*, 120–125.

723 Garcia, H.G., Tikhonov, M., Lin, A., and Gregor, T. (2013). Quantitative imaging of
724 transcription in living Drosophila embryos links polymerase activity to patterning. Curr. Biol.
725 *23*, 2140–2145.

726 Gregor, T., Tank, D.W., Wieschaus, E.F., and Bialek, W. (2007a). Probing the Limits to
727 Positional Information. Cell *130*, 153–164.

728 Gregor, T., Wieschaus, E.F., McGregor, A.P., Bialek, W., and Tank, D.W. (2007b). Stability
729 and Nuclear Dynamics of the Bicoid Morphogen Gradient. Cell *130*, 141–152.

730 Guglielmi, G., Barry, J.D., Huber, W., and De Renzis, S. (2015). An Optogenetic Method to
731 Modulate Cell Contractility during Tissue Morphogenesis. Dev. Cell.

732 Gurdon, J.B., and Bourillot, P.Y. (2001). Morphogen gradient interpretation. Nature *413*,
733 797–803.

734 Harfe, B.D., Scherz, P.J., Nissim, S., Tian, H., McMahon, A.P., and Tabin, C.J. (2004).
735 Evidence for an expansion-based temporal Shh gradient in specifying vertebrate digit
736 identities. Cell *118*, 517–528.

Hoch, M., Seifert, E., and Jäckle, H. (1991). Gene expression mediated by cis-acting sequences of the Krüppel gene in response to the Drosophila morphogens bicoid and hunchback. EMBO J. *10*, 2267–2278.

Hülskamp, M., Pfeifle, C., and Tautz, D. (1990). A morphogenetic gradient of hunchback protein organizes the expression of the gap genes Krüppel and knirps in the early Drosophila embryo. Nature *346*, 577–580.

Jaeger, J., Surkova, S., Blagov, M., Janssens, H., Kosman, D., Kozlov, K.N., Manu, Myasnikova, E., Vanario-Alonso, C.E., Samsonova, M., et al. (2004). Dynamic control of positional information in the early Drosophila embryo. Nature *430*, 368–371.

Johnson, H.E., Goyal, Y., Pannucci, N.L., Schüpbach, T., Shvartsman, S.Y., and Toettcher, J.E. (2017). The Spatiotemporal Limits of Developmental Erk Signaling. Dev. Cell *40*, 185–192.

Kennedy, M.J., Hughes, R.M., Peteya, L. a, Schwartz, J.W., Ehlers, M.D., and Tucker, C.L. (2010). Rapid blue-light-mediated induction of protein interactions in living cells. Nat. Methods *7*, 973–975.

Kraut, R., and Levine, M. (1991). Spatial regulation of the gap gene giant during Drosophila development. *609*.

Little, S.C., Tkačik, G., Kneeland, T.B., Wieschaus, E.F., and Gregor, T. (2011). The formation of the bicoid morphogen gradient requires protein movement from anteriorly localized mRNA. PLoS Biol. *9*.

Liu, F., Morrison, A.H., and Gregor, T. (2013). Dynamic interpretation of maternal inputs by the Drosophila segmentation gene network. Proc. Natl. Acad. Sci. U. S. A. *110*, 6724–6729.

Lucas, T., Ferraro, T., Roelens, B., De Las Heras Chanes, J., Walczak, A.M., Coppey, M., and Dostatni, N. (2013). Live Imaging of Bicoid-Dependent Transcription in Drosophila Embryos. Curr. Biol. *23*, 2135–2139.

Lucchetta, E.M., Lee, J.H., Fu, L.A., Patel, N.H., and Ismagilov, R.F. (2005). Dynamics of Drosophila embryonic patterning network perturbed in space and time using microfluidics. Nature *434*, 1134–1138.

Manu, Surkova, S., Spirov, A., Gursky, V., Janssens, H., Kim, A.-R., Radulescu, O., Vanario-Alonso, C.E., Sharp, D.H., Samsonova, M., et al. (2009). Canalization of Gene Expression in the Drosophila Blastoderm by Gap Gene Cross Regulation. PLoS Biol. *7*, e1000049.

Martin, A.C., Gelbart, M., Fernandez-Gonzalez, R., Kaschube, M., and Wieschaus, E.F. (2010). Integration of contractile forces during tissue invagination. J. Cell Biol. *188*, 735–749.

Neumann, C., and Cohen, S. (1997). Morphogens and pattern formation. Bioessays *19*, 721–729.

Perry, M.W., Boettiger, A.N., and Levine, M. (2011). Multiple enhancers ensure precision of gap gene-expression patterns in the Drosophila embryo. Pnas *108*, 1–12.

Perry, M.W., Bothma, J.P., Luu, R.D., and Levine, M. (2012). Precision of hunchback expression in the Drosophila embryo. Curr. Biol. *22*, 2247–2252.

Sako, K., Pradhan, S.J., Barone, V., Inglés-Prieto, Á., Müller, P., Ruprecht, V., Čapek, D., Galande, S., Janovjak, H., and Heisenberg, C.-P. (2016). Optogenetic Control of Nodal Signaling Reveals a Temporal Pattern of Nodal Signaling Regulating Cell Fate Specification during Gastrulation. Cell Rep. 866–877.

Sander, K. (1976). Specification of the Basic Body Pattern in Insect Embryogenesis. Adv. In Insect Phys. *12*, 125–238.

Sommer, C., Straehle, C., Ullrich, K., and Hamprecht, F. a (2011). Ilastik: Interactive learning and segmentation toolkit. Eighth IEEE Int. Symp. Biomed. Imaging 230–233.

Stanojevic, D., Small, S., and Levine, M. (2016). Regulation of a Segmentation Stripe by Overlapping Activators and Repressors in the Drosophila Embryo. *254*, 1385–1387.

Struhl, G., Struhl, K., and Macdonald, P.M. (1989). The gradient morphogen bicoid is a concentration-dependent transcriptional activator. Cell *57*, 1259–1273.

Tucker, J.A., Mintzer, K.A., and Mullins, M.C. (2008). The BMP Signaling Gradient Patterns Dorsoventral Tissues in a Temporally Progressive Manner along the Anteroposterior Axis. Dev. Cell *14*, 108–119.

Turing, A.M. (1990). The chemical basis of morphogenesis. Bull. Math. Biol. *52*, 153–197.

Venken, K.J.T., Schulze, K.L., Haelterman, N. a, Pan, H., He, Y., Evans-Holm, M., Carlson, J.W., Levis, R.W., Spradling, A.C., Hoskins, R. a, et al. (2011). MiMIC: a highly versatile transposon insertion resource for engineering Drosophila melanogaster genes. Nat. Methods *8*, 737–743.

Verd, B., Crombach, A., and Jaeger, J. (2017). Dynamic Maternal Gradients Control Timing and Shift-Rates for Drosophila Gap Gene Expression. PLoS Comput. Biol. *13*, e1005285.

Vincent, A., Blankenship, J.T., and Wieschaus, E. (1997). Integration of the head and trunk segmentation systems controls cephalic furrow formation in Drosophila. Development *124*, 3747–3754.

Wolpert, L. (1969). Positional information and the spatial pattern of cellular differentiation. J. Theor. Biol. *25*, 1–47.

Supplementary material 1. Quantification of MS2 RNA reporter

Nascent hb transcripts were detected from live-imaging data using both ImageJ[1] and Matlab.

Image processing in ImageJ

Each Z-stack for each time point was Z-projected (maximum intensity). In order to automate the tracking and subsequent analysis, the following parameters were manually measured from the projections: lowest intensity value, spot size (matrix size, $N \times N$), maximum displacement distance within two frames and intensity difference between MS2 dots and surrounding background.

Automation, tracking and analysis in Matlab

The embryo boundary was automatically traced and extracted from projected images by using the 'bwboundaries' function[2]. This measurement was later used to exclude false positive and to calculate the coordinates for each MS2 dots. At each time frame, MS2 dots were localized by applying a threshold corresponding to the lowest intensity value. Pixels showing an intensity higher than this threshold were selected. Following the selection, the pixels out of the embryo boundary were excluded. Next, a regional intensity comparison was performed by comparing the intensity of the selected pixels to its surrounding pixels within a $(N+2)\times(N+2)$ matrix window. The intensity difference between the selected pixel and the average intensity of its neighbours was calculated and pixels having a value higher than the approximate intensity difference between MS2 dots and surrounding background were selected. Central coordinates, averaged intensity value and AP position were recorded for subsequent quantification. Tracking of MS2 dots used the maximum MS2 dots displacement distance calculated above to define a displacement range. Hence, a MS2 dot at the frame t was connected to the nearest dot at the frame t+1 within the displacement range. Last, we excluded dot tracks lasting less than 160s as it is shorter than a complete hb transcription event. The probability distribution of MS2 dots persistence in the anterior and posterior domains was calculated. The anterior domain was subdivided into 5 regions (100-75, 75-70, 70-65, 65-60 and 60-40 %EL) to refine the analysis.

1. Schindelin, J. *et al*. Fiji: an open-source platform for biological-image analysis. *Nat. Methods* **9,** 676–682 (2012).

2. Gonzalez, R. C., R. E. Woods, and S. L. Eddins, *Digital Image Processing Using MATLAB*, New Jersey, Pearson Prentice Hall (2004).